Tilted excitation implies odd periodic resonances

G. I. Depetri,[1,2,*] J. C. Sartorelli,[2,†] B. Marin,[2,3] and M. S. Baptista[4]

[1]*Instituto de Física "Gleb Wataghin," Universidade Estadual de Campinas, 13083-859 Campinas, SP, Brazil*

[2]*Instituto de Física da Universidade de São Paulo, 05315-970 São Paulo, SP, Brazil*

[3]*Department of Neuroscience, Physiology and Pharmacology, University College London, Gower Street, London WC1E 6BT, United Kingdom*

[4]*Institute for Complex Systems and Mathematical Biology, SUPA, University of Aberdeen, Aberdeen AB24 3UE, United Kingdom*

(Received 22 January 2016; published 5 July 2016)

Our aim is to unveil how resonances of parametric systems are affected when symmetry is broken. We showed numerically and experimentally that odd resonances indeed come about when the pendulum is excited along a tilted direction. Applying the Melnikov subharmonic function, we not only determined analytically the loci of saddle-node bifurcations delimiting resonance regions in parameter space but also explained these observations by demonstrating that, under the Melnikov method point of view, odd resonances arise due to an extra torque that appears in the asymmetric case.

DOI: 10.1103/PhysRevE.94.012202

I. INTRODUCTION

Resonance is a ubiquitous phenomenon. It provides an ideal landscape for efficient functioning of many natural and technological systems, such as the amplification of speech in body cavities [1], the motion of a child on a swing [2], imaging by magnetic resonance, and electronic signal amplification [3–5]. Parametric resonance, in particular, arises from time-dependent modulation of system parameters and has important implications in phenomena ranging from boat capsizing in naval engineering [6], encoding of tactile information in rodent whisking behavior [7], and energy harvesting from mechanical oscillatory motion [8]. The parametric pendulum, described by

$$\ddot{\theta} + \beta\dot{\theta} + (1 + P\cos\Omega_p t)\sin\theta = 0, \tag{1}$$

is a paradigmatic model in nonlinear dynamics [9–11]. It consists of a planar simple pendulum whose pivot oscillates harmonically along the vertical direction with amplitude P and frequency Ω_p, and β is the friction parameter. This system has attracted great attention [12–17]. It presents a wide range of dynamical behavior, such as the stabilization of the hilltop saddle [18–23], the occurrence of chaotic behavior [24–29], the observation of period-doubling cascades [30,31], and the existence of resonance regions [11,32]. Moreover, it can be used as a qualitative analog for more complex systems [31,33,34]. Indeed, mechanical analogs of physical systems provide a direct visualization of motion, allowing an intuitive understanding of the system being studied, as is done for the analysis of power grid [35] and applications of telecommunications [36]. Rotating motion in the parametric pendulum has also been widely considered in the literature [37], due to the possibility of energy harvesting from sea waves, which would consist in transforming the vertical motion of sea waves in rotating motion of systems composed by parametric pendula [8,38–41].

The study of stable periodic orbits of Eq. (1) has a long academic history, in particular regarding those whose period is an even or odd multiple of the excitation period [42]. Previous works show the existence of both even [30,43] and odd [31,44,45] oscillations in the frequency region $\Omega_p < 2$. Odd resonances, however, are very rarely reported, supposedly due to its nontypical nature (only observed for narrow ranges of parameter values, according to Ref. [44]). To describe theoretically the mechanisms that could lead to subharmonic solutions, Koch and Leven [46] applied the Melnikov theorem for subharmonic bifurcations [47,48] to this system. They succeeded in calculating parameter ranges for the existence of even oscillations but concluded that the Melnikov theorem could not be applied to unravel parameter ranges for odd oscillations. This is also true when the Melnikov method is applied to other similar parametric systems [49–51]. In Ref. [52], it is shown that for nonlinear perturbed systems, even oscillations are due to parametric excitation along the gravitational field, while odd oscillations can exist as consequence of external torques. Looking at Eq. (1), one notices that this system is symmetric with respect to the transformation $\theta \to -\theta$. External torques are absent. However, breaking the symmetry of Eq. (1) by a tilt in the pendulum pivot motion should introduce an additional torque in the equations of motion, as we shall see. A question then arises: Does symmetry breaking affect somehow the behavior of odd oscillations?

We have demonstrated numerically and experimentally, for the tilted parametric pendulum, the existence of odd resonances in the frequency region $\Omega_p > 2$. Also, applying the Melnikov subharmonic function, we obtained analytically the loci of saddle-node bifurcations that are the parameter thresholds for the existence of odd stable oscillations. Surprisingly, these loci coincide with the curves that limit resonance regions found numerically. Moreover, we show that according to the Melnikov method approach, whereas even resonances are a consequence of the vertical excitation, odd ones comes about due to the tilt in the orientation of the excitation with respect to the vertical position. This work therefore paves the way to a better understanding of how resonances of any type can appear in complex oscillating systems and how they can be related to symmetry.

II. EXPERIMENTAL APPARATUS

A diagram of the experimental apparatus is shown in Fig. 1. The pendulum consists of a single arm with mass m and center-of-mass position at a distance l from the pivot axis. The natural

*gdepetri@if.usp.br

†sartorelli@if.usp.br

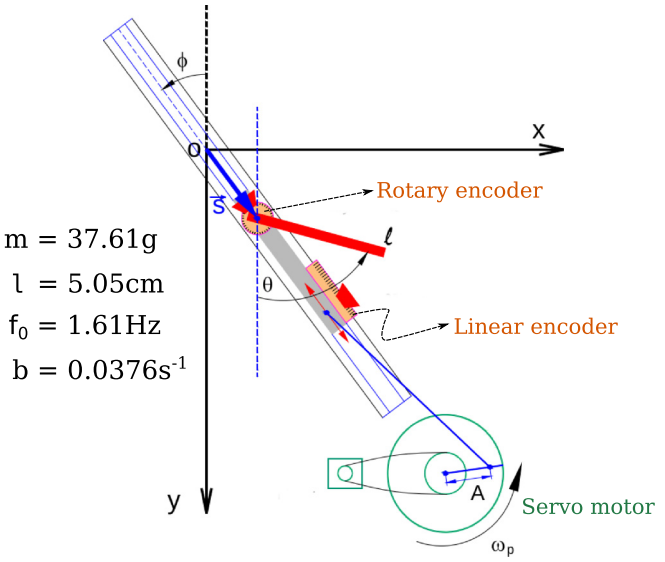

FIG. 1. Diagram of the experimental apparatus of a planar simple pendulum parametrically excited along an arbitrary direction. The pendulum pivot axis is attached to a sliding car that is forced to oscillate with amplitude A and frequency f_p, with the help of a crank and a servo motor. We can measure simultaneously the absolute value of the pivot speed v_p, with a linear encoder system in the laboratory reference frame, and the absolute value of the pendulum angular velocity $|\omega|$, with a rotary encoder system attached to the pendulum.

frequency of oscillation is f_0 and the friction parameter is b [53]. The angle between the pendulum arm and the vertical direction is θ. The pivot of the pendulum is attached to a sliding car, which is periodically excited according to $s = A\cos\omega_p t$, along a tilted axis making an angle $\phi = \pi/8$ with the vertical direction. The rail over which the pivot oscillates is attached to the wall; therefore ϕ is not a dynamic parameter. To measure the absolute value of the pivot velocity $v_p = |\dot{s}|$, we attached a linear optical encoder, of resolution $\frac{2.54}{500}$ cm, to the sliding car. From the time series $v_p(t)$, we can obtain the frequency $f_p = 2\pi\omega_p$ and the amplitude A of the external excitation, which are the control parameters of the system.

To measure the absolute value of the angular velocity $\omega = \dot{\theta}$ of the pendulum arm, we attached an optical rotary encoder, of resolution $\frac{2\pi}{2500}$ rad, to the pendulum arm, concentric to the pivot point. The light sensor of the rotary encoder is attached to the sliding car, concentrically to the pivot, while the sensor of the linear encoder is attached to the laboratory reference frame. The induced inputs from both encoders were detected by using an Analog Digital Converter (ADC) board of 16 bits at the rate of 200 Ksamples/s. For fixed values of A, the excitation frequency f_p was spanned in the forward and backward directions with a servo motor in steps of 0.01 Hz.

III. EQUATIONS OF MOTION

The equations of motion of the undamped parametric pendulum can be obtained via Lagrangian formulation. Adding a linear damping term $-b\dot{\theta}$, we arrive at

$$\dot{\theta} = \omega,$$
$$\dot{\omega} = -\sin\theta - [P\cos(\Omega_p\bar{t})\sin(\theta-\phi) + \beta\omega], \qquad (2)$$

where the dot indicates derivative with respect to the normalized time $\bar{t} = \omega_0 t$, and

$$\Omega_p = \frac{\omega_p}{\omega_0}, \quad P = \frac{\omega_p^2 A}{g}, \quad \beta = \frac{b}{\omega_0}, \qquad (3)$$

are the dimensionless parameters of the system. The period of the perturbation is $T_p = 2\pi/\Omega_p$. Notice the symmetry $\theta \to -\theta$ is now broken, and comparing with Eq. (1) we have an extra torque given by $\tau = P\sin\phi\cos(\Omega_p\bar{t})\cos\theta$, non-null for $\phi \neq 0$.

IV. DATA ANALYSIS

The periodicity of each trajectory, both in numerical and experimental analysis, was computed from the stroboscopic map for the absolute value of the angular velocity of the pendulum $|\omega[(k+1)T_p]| \times |\omega(kT_p)|$, $k \in \mathbb{N}$. The stroboscopic map is obtained by observing the (absolute) values of the pendulum velocity $|\omega(t)|$ every time the perturbation completes a full cycle, i.e., every second maximum of v_p. In Fig. 2, sampled experimental time series for period-2, -3, -4, and -5 oscillations are displayed, as well as the respective stroboscopic maps. The number of points m in the stroboscopic map is related to the ratio between the period of oscillation and the period of the excitation, being that $T/T_p = m/n$, with m and n coprime integers.

V. NUMERICAL RESULTS

In Fig. 3 parameter spaces for the symmetric (a) and asymmetric (b) cases are shown. They are constructed using direct integration. For each pair of parameters (Ω_p, P) we integrate Eqs. (2) for a time span $\bar{t} = 1000$, with initial conditions $\theta_i = 0.55$ and $\omega_i = 0$ and, after discarding initial data up to $\bar{t} = 900$ (transient behavior), we compute the periodicity of the stationary solution as explained in Sec. IV. Rotations and oscillations of different periods, as well as irregular motion, are observed.

In Fig. 3(a), we display the parameter space for the vertical excitation case. Notice that off the resonance regions, the pendulum does not oscillate but stays at the fixed point (FP) $\theta = \omega = 0$. From the right to the left, full line SN4 is the loci of saddle-node bifurcations for which a period-4 stable oscillations (P4) come about, and full line PK is the loci of pitchfork bifurcations at which stable period-2 (P2) oscillations appear. Then we have period-1 (R1) and period-2 (R2) rotations and persistent tumbling chaos (CH). In Fig. 3(b) we have the parameter space for the nonsymmetric perturbation case. Regions P1 represent parameters generating nonresonant regions, when the pendulum oscillates with the same period of the perturbation. From the right to the left, we see with the full lines SN4, SN3, and SN5/2, respectively, the loci of saddle-node bifurcations from which period-4 (P4), period-3 (P3), and period-5/2 stable oscillations come about. Full line PD is the loci of period-doubling bifurcations in which the period-1 oscillations lose stability and stable period-2 resonant stable oscillations (P2) appear. We observe period-1 (R1) and period-2 (R2) rotations, and then persistent tumbling chaos (CH). Multistability is present for some parameter values, but since the integration has only been performed for a

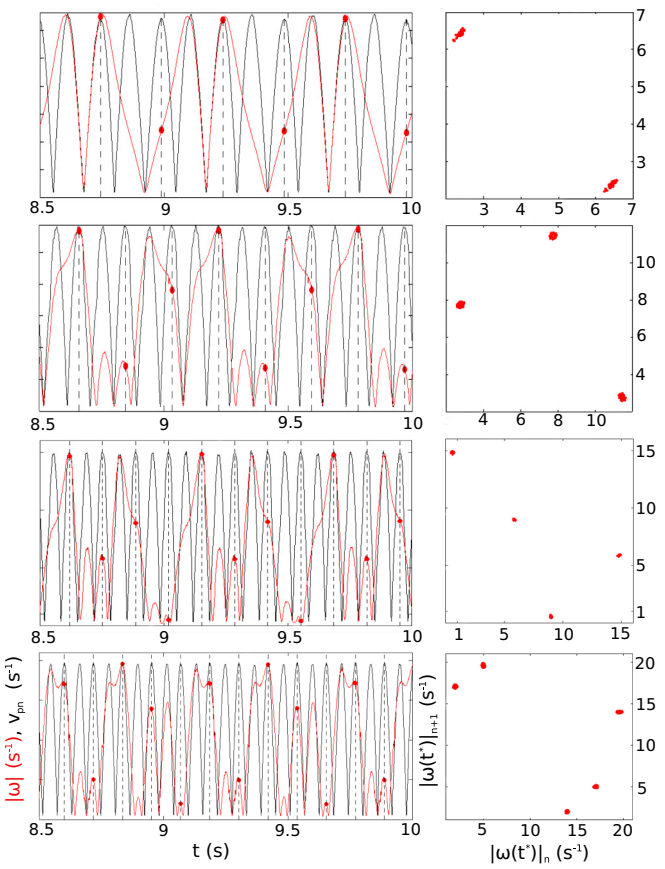

FIG. 2. On the left column, from the top to the bottom, we display sampled experimental time series for fixed amplitude $A = 2.02$ cm illustrating period-2 ($f_p = 4.05$ Hz), period-3 ($f_p = 5.35$ Hz), period-4 ($f_p = 7.5$ Hz), and period-5 ($f_p = 8.55$ Hz) oscillations. Full red lines represent the modulus of the pendulum angular velocity, $|\omega|$, and full black lines the time series for the modulus of perturbation velocity normalized with respect to the maximum value of $|\omega|$, v_{pn}. Full red circles are the values of the pendulum velocity each time the perturbation completes a full cycle. On the right column we have the corresponding stroboscopic maps for each time series.

single initial condition, this cannot be seen here. In the vertical case we observed only even resonances and in the tilted case, both even and odd resonances. However, we must have in mind that the parameter space depends on the choice of initial conditions.

For the parametrically excited double pendulum, regions of nonoscillation and the pitchfork bifurcations in the vertical case are substituted for period-1 oscillations and period-doubling bifurcations when excitation is tilted [57,58]. This is due to the extra torque introduced by symmetry breaking, as seen in Sec. III.

VI. EXPERIMENTAL RESULTS

We confirm experimentally the behaviors in Fig. 3(b) through bifurcation diagrams by fixing the amplitude of excitation at $A = 2.02$ cm and performing both forward and backward frequency sweeps. Results are shown on Fig. 4(a). The occurrence of odd primary resonances P1, P3, and P5

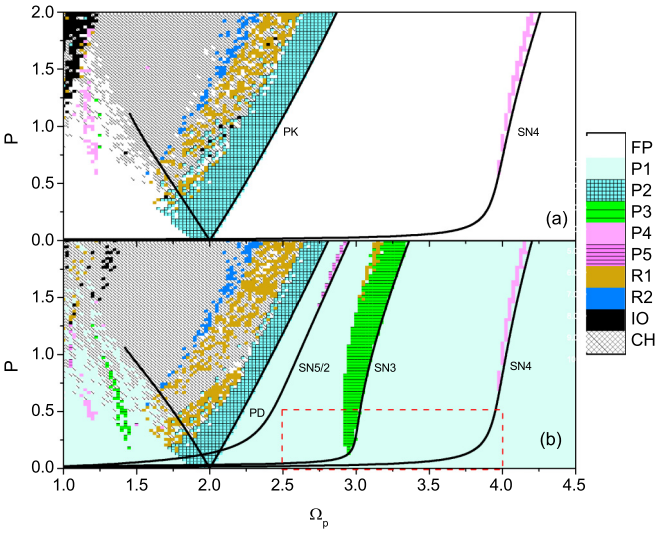

FIG. 3. Parameter spaces for (a) vertical ($\phi = 0$) and (b) tilted ($\phi = \pi/8$) excitations. FP denotes fixed point; Pm and Rm, period-m [42] oscillation and rotation, respectively; IO periodic inverted oscillations; and CH persistent tumbling chaos [27]. Full lines represent the loci of saddle-node (SN), pitchfork (PK), and period-doubling (PD) bifurcations and were obtained with the software AUTO 07p [54,55]. See the Supplemental Material for the numerical code [56].

for large parameter ranges is remarkable. It is important to observe that the control parameter in the laboratory are the amplitude A and the frequency f_p of the excitation, while the parameter space is computed in terms of the normalized parameters P and Ω_p. Since $P = \frac{\omega_0^2}{g} A\Omega_p^2$, by keeping A constant, we have a parabola in the parameter space of Fig. 3.

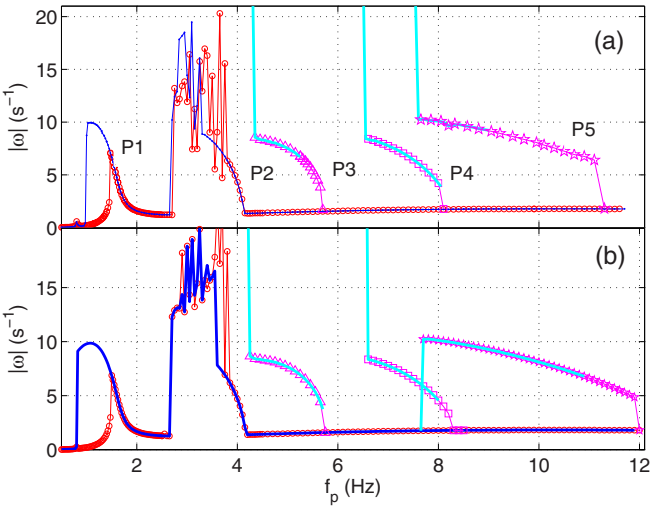

FIG. 4. Bifurcation diagrams at $A = 2.02$ cm obtained (a) experimentally and (b) numerically. Frequency of the excitation was spanned both forward (line with empty circles) and backwards (full line). Periodic oscillations P3, P4, and P5 are excited by manually setting up initial conditions of the pendulum and are displayed in triangles, squares, and stars, respectively, for forward frequency sweeping and in full lines for backward sweeping.

Also, all points in parameter space are generated by integrating the equations of motion with the same initial conditions. When the experiment is being performed, the initial conditions are automatically updated from point to point. To show the remarkable agreement between numeric and experimental results, in Fig. 4(b) we show the equivalent bifurcation diagram computed numerically.

Along the line with empty circles (increasing f_p), from the left to the right, the pendulum starts realizing small oscillations with the same period and phase of the excitation. At $f_p = \frac{f_0}{2} = 0.8$ Hz, we have a bifurcation at which it oscillates with period $\frac{T_p}{2}$ and out of phase with perturbation. Another bifurcation happens at around $f_p = f_0 = 1.61$ Hz, causing it to oscillate with the same period of the perturbation but with a different phase. For larger frequencies, at around $f_p = 2$ Hz, the pendulum slowly gets in phase with the excitation. For around $f_p = 2.8$ Hz irregular motion is observed and we needed to prevent the pendulum from rotating, because the energy gain is so large that it can destroy the apparatus [57]. Around $f_p = 2f_0 = 3.22$ Hz the pendulum oscillates with twice the period of excitation, and for a slight increase in frequency it goes back to oscillating with the same period and phase of the perturbation until the end of data acquisition. Following the full line (decreasing f_p), we observe basically the same phenomena, except for when there is hysteresis. In this process, we observe no oscillation with period higher than $2T_p$, but this is because in the frequency region where we expect to observe those solutions, the pendulum is oscillating in the regime of small oscillations, outside the basins of attraction of these long-period attractors.

To detect those solutions, we need to manually adjust the initial conditions of the pendulum in the parameter region in which we expect to observe them. Then, once the wanted attractor is found, we perform forward and backward frequency sweeps. If we adjust $\theta_0 \approx 0.5$ in the region $f_p \approx 3f_0 = 4.83$ Hz, then we find the period-3 resonant oscillatory attractor P3. The triangles represent those solutions with increasing frequency, and the full line above them the same solutions with decreasing frequency. Also, if we adjust $\theta_0 \approx 0.36$ in the region $f_p \approx 4f_0 = 6.44$ Hz, we find the period-4 oscillatory attractor P4. The squares represent those solutions with increasing frequency and, as before, the full line above them, the same solutions with decreasing frequency. We also found period-5 oscillations we did not foresee numerically from Fig. 3, because the initial conditions we chose were out of its basin of attraction. If we adjust $\theta_0 \approx 0.9$ in the region $f_p \approx 5f_0 = 8.05$ Hz, then we will find attractor P5, which is represented by stars in the case of increasing frequency and by a full line above them in the case of decreasing frequency. In Fig. 4(a) all full lines represent pendulum behavior that for a decreasing frequency go into rotating motion, resulting in an abrupt increase in $|\omega|$. In Fig. 4(b) this is not always the case; for P5, at $f_p = 7.7$ Hz, it ends up going back to period-1 oscillations. This difference can be explained by the coexistence of periodic rotations and oscillations. The coexistence of period-1, period-4, and period-5 oscillatory attractors in the small range $7.8 < f_p < 8.05$ Hz is noteworthy. See the Supplemental Material for videos illustrating this triple coexistence [56].

VII. MELNIKOV SUBHARMONIC FUNCTION

Parameter thresholds for the occurrence of resonant periodic oscillations are derived by applying the Melnikov method for subharmonic solutions. The planar simple pendulum is described by the (Hamiltonian) vector field $f(\theta,\omega) = [\omega \;\; -\sin(\theta)]^\intercal$. The phase space has a pair of homoclinic orbits biasymptotic to the saddle points $(\theta,\omega) = (\pm\pi,0)$, and their interior is filled by a continuous family of periodic oscillations $q^\alpha(t) = (\theta^\alpha(t),\omega^\alpha(t))$, with α being a label, described by

$$\cos\left(\frac{\theta^\alpha}{2}\right) = k\,\mathrm{sn}(t,k), \quad \sin\left(\frac{\theta^\alpha}{2}\right) = \mathrm{dn}(t,k), \qquad \omega^\alpha = \dot{\theta}^\alpha = 2k\,\mathrm{cn}(t,k), \tag{4}$$

where $\mathrm{sn}(t,k)$, $\mathrm{cn}(t,k)$, and $\mathrm{dn}(t,k)$ are the Jacobi elliptic functions and $k \in [0,1]$ is the elliptic modulus [59]. The period of these solutions is $T_\alpha = 4K(k)$, where $K(k)$ is the complete elliptic integral of first kind. Now we perturb this system with the time-dependent and periodic (of period $T_p = 2\pi/\Omega_p$) vector field $g(\theta,\omega,P,\Omega_p,\beta) = [0 \;\; -\epsilon P\cos(\Omega_p\tau)\sin(\theta-\phi) - \beta\omega]^\intercal$, with $0 < \epsilon \ll 1$ and consider the quantity

$$M^m(t_0) = \int_0^{mT_p} -\omega^\alpha(t)[P\cos\Omega_p t\sin(\theta^\alpha - \phi) - \beta\omega^\alpha]dt, \tag{5}$$

which is a path integral computed along the periodic oscillation $q^\alpha(t)$ of period $T_\alpha = mT_p$, that is, a solution satisfying the resonance condition

$$4K(k) = m\frac{2\pi}{\Omega_p}. \tag{6}$$

Theorem 4.6.2 of Ref. [47] states that if $M^m(t_0)$ has simple zeros, meaning $M^{m/n}(t_0) = 0$, but $\frac{\partial M^{m/n}}{\partial t_0}(t_0) \neq 0$, then the perturbed system has a solution that is a periodic subharmonic oscillation of period mT_p, arising from a saddle-node bifurcation.

Substituting Eqs. (4), subject to the resonance condition (6), into Eq. (5), we have

$$M^m(t_0) = -4k^2\beta I_1 - 4k^2 P\cos\phi I_2 + 2kP\sin\phi I_3 - 4k^3 P\sin\phi I_4, \tag{7}$$

where

$$I_1 = \int_0^{mT_p} \mathrm{cn}^2(t,k)dt,$$

$$I_2 = \int_0^{mT_p} \cos[\Omega_p(t+t_0)]\mathrm{cn}(t,k)\mathrm{sn}(t,k)\mathrm{dn}(t,k)dt,$$

$$I_3 = \int_0^{mT_p} \cos[\Omega_p(t+t_0)]\mathrm{cn}(t,k)dt,$$

$$I_4 = \int_0^{mT_p} \cos[\Omega_p(t+t_0)]\mathrm{cn}(t,k)\mathrm{sn}^2(t,k)dt.$$

Imposing $M^m(t_0)$ has simple zeros and we obtain the loci of the saddle-node bifurcations generating a subharmonic resonant periodic orbit, i.e., the minimum values R^m such that for $P > R^m$ we might observe stable oscillatory motion of period mT_p in the parameter space.

If m is even, then $I_3 = I_4 = 0$, and $M^m(t_0)$ can only have simple zeros if I_2, which comes from the vertical excitation

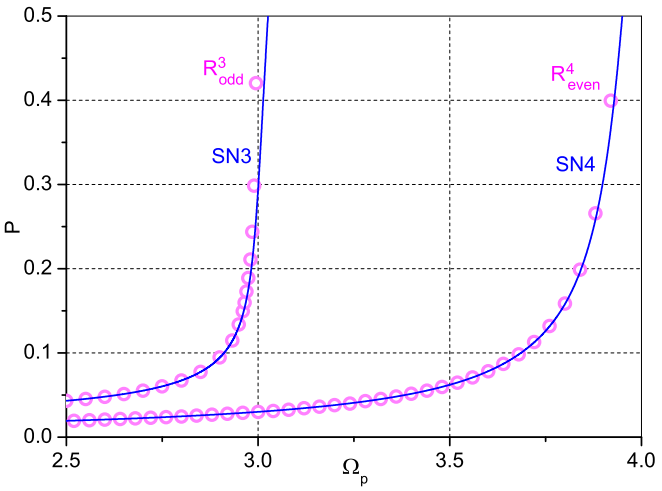

FIG. 5. A zoom into the parameter space of the tilted parametric pendulum, representing the red dashed rectangle region indicated in Fig. 3. Melnikov thresholds R^3_{odd} and R^4_{even} (empty circles) agree finely with the borders of resonance regions SN3 and SN4 (full lines), respectively.

component, is nonidentically null. In this case, R^m_{even} is given by

$$R^m_{\text{even}}(\Omega_p) = \frac{4\beta[E(k) - k'^2 K(k)]}{\pi \cos\phi \Omega_p^2} \sinh[\Omega_p K'(k)], \qquad (8)$$

where $k'^2 = 1 - k^2$ is the complementary elliptic modulus and $K'(k) = K(k')$. On the other hand, if m is odd, $I_2 = 0$, and $M^m(t_0)$ can only have simple zeros if I_3 or/and I_4, which are both due to the additional torque τ caused by the tilt in the pivot motion, are nonidentically null. Then, R^m_{odd} is given by

$$R^m_{\text{odd}}(\Omega_p) = \frac{4\beta[E(k) - k'^2 K(k)]}{\pi \sin\phi \left\{\left[\frac{2E(k)}{K(k)} - 1\right]\text{sech}(\Omega_p K'(k)) + \frac{\pi^2 S}{K^2(k)}\right\}}, \qquad (9)$$

where

$$S = \sum_{l=0}^{\infty} \frac{a_+(l)}{2} \text{csch}\left[\frac{a_+(l)}{m}\Omega_p K'(k)\right] \text{sech}\left[\frac{b(l)}{m}\Omega_p K'(k)\right] + \sum_{\substack{l=0 \\ l \neq \frac{m-1}{2}}}^{\infty} \frac{a_-(l)}{2} \text{csch}\left[\frac{a_-(l)}{m}\Omega_p K'(k)\right] \text{sech}\left[\frac{b(l)}{m}\Omega_p K'(k)\right],$$

with $a_+(l) = 2l + 1 + m$, $a_-(l) = 2l + 1 - m$, and $b(l) = 2l + 1$.

The elliptic modulus k is determined from Ω_p through the resonance condition, and it is worth noticing that for $\Omega_p > m$ there is no k such that Eq. (6) is satisfied. It is remarkable that for the vertically excited pendulum we have $\sin\phi = 0$, and no Melnikov condition for the existence of odd oscillations can be determined, that is, $M^m(t_0)$ does not have simple zeros in this case.

In Fig. 5 we see remarkable agreement between numeric and analytic predictions for the loci of the saddle-node bifurcations where the oscillatory resonant stable periodic attractors P3 and P4 appear in the region $P < 0.5$. Full lines SN3 and SN4 were obtained with AUTO [54,55] (see Fig. 3), and circles indicated by R^3_{odd} and R^4_{even} represent $\{R^3_{\text{odd}} \times \Omega_p\}$ and $\{R^4_{\text{even}} \times \Omega_p\}$ respectively. Therefore, the minimal value of P analytically calculated by the Melnikov method provides the parameter values for the onset of these resonances.

VIII. CONCLUSIONS

The novelty was to show that odd resonant oscillations are likely to be observed in the tilted parametric pendulum, enlarging the spectra of possible resonances in the system. The occurrence of odd resonances when excitation is along a tilted direction was explained by the Melnikov subharmonic function. We not only demonstrated that the loci of saddle-node bifurcations that is the threshold obtained by application of this method excellently agrees with those computed using numeric continuation technique, which implies that primary resonances are indeed described by this method, but also showed that, according to this approach, whereas even resonances are due to the vertical excitation component, odd resonances are a result of an extra torque that appears only in the tilted case, as a consequence of the symmetry breaking of the equations of motion.

ACKNOWLEDGMENTS

This work was supported by the Brazilian agencies FAPESP (2011/19296-1) and CNPq (307947/2014-9). M.S.B. also acknowledges the EPSRC Ref: EP/I032606/1. G.I.D. thanks Felipe A. C. Pereira for fruitful discussions.

[1] E. Joliveau, J. Smith, and J. Wolfe, Nature **427**, 116 (2004).
[2] W. Case and M. Swanson, Am. J. Phys. **58**, 463 (1990).
[3] D. P. Howson and R. B. Smith, *Parametric Amplifiers*, 1st ed. (McGraw-Hill, New York, 1970).
[4] J. Hansryd, P. A. Andrekson, M. Westlund, J. Li, and P. Hedekvist, IEEE J. Sel. Topics Quantum Eletron. **8**, 506 (2002).
[5] K. K. Likharev, *Dynamics of Josephson Junctions and Circuits*, 1st ed. (CRC Press, Boca Raton, FL 1986).
[6] C. Holden, R. Galeazzi, C. Rodríguez, T. Perez, T. I. Fossen, M. Blanke, and M. A. S. eida Neves, Model. Ident. Control **28**, 87 (2007).
[7] T. Volkova, I. Zeidis, H. Witte, M. Schmidt, and K. Zimmermanna, J. Bionic. Eng. **13**, 312 (2016).
[8] B. W. Horton and M. Wiercigroch, *IUTAM Symposium on Fluid-Structure Interaction in Ocean Engineering*, edited by E. Kreutzer, (Springer, Netherlands, 2008), Vol. 8, pp. 117–128.

[9] Ignoring friction, in the small amplitude regime the differential equation for the angle displacement θ of the pendulum arm is the Mathieu equation [10], from which many properties are known.

[10] L. Ruby, Am. J. Phys. **64**, 39 (1996).

[11] E. Butikov, J. Phys. A: Math. Gen. **35**, 6209 (2002).

[12] A. S. de Paula, M. A. Savi, M. Wiercigroch, and E. Pavlovskaia, Int. J. Bifurcat. Chaos **22**, 1250111 (2012).

[13] B. Horton, J. Sieber, J. M. T. Thompson, and M. Wiercigroch, Int. J. Nonlinear Mech. **46**, 436 (2011).

[14] S. Lenci and S. Rega, J. Comput. Nonlinear Dyn. **3**, 041010 (2008).

[15] Xu Xu and M. Wiercigroch, Nonlinear Dyn. **47**, 311 (2007).

[16] J. L. Trueba, J. P. Baltanás, and M. A. F. Sanjuán, Chaos Soliton. Fract. **15**, 911 (2003).

[17] S. R. Bishop, D. L. Xu, and M. J. Clifford, Proc. R. Soc. A **452**, 1789 (1996).

[18] A. Stephenson, Philos. Mag. S. 6 **15**, 233 (1908).

[19] H. J. T. Smith and J. A. Blackburn, Am. J. Phys. **60**, 909 (1992).

[20] D. J. Acheson, Proc. R. Soc. A **448**, 89 (1995).

[21] M. J. Clifford and S. R. Bishop, Proc. R. Soc. A **454**, 2811 (1998).

[22] S. R. Bishop and D. J. Sudor, Int. J. Bifurcat. Chaos **09**, 273 (1999).

[23] E. Butikov, Am. J. Phys. **69**, 755 (2001).

[24] R. W. Leven and B. P. Koch, Phys. Lett. A **86**, 71 (1981).

[25] B. P. Koch, R. W. Leven, B. Pompe, and C. Wilke, Phys. Lett. A **96**, 219 (1983).

[26] R. W. Leven, B. Pompe, C. Wilke, and B. P. Koch, Physica D **16**, 371 (1985).

[27] S. R. Bishop and M. J. Clifford, J. Sound Vib. **189**, 142 (1996).

[28] W. Szemplińska-Stupnicka, E. Tyrkiel, and A. Zubrzycki, Int. J. Bifurcat. Chaos **10**, 2161 (2000).

[29] W. Szemplińska-Stupnicka and E. Tyrkiel, Nonlinear Dynam. **27**, 271 (2003).

[30] J. McLaughlin, J. Stat. Phys. **24**, 375 (1981).

[31] A. Arneodo, P. Coullet, C. Tresser, A. Libchaber, J. Maurer, and D. d'Humiéres, Physica D **6**, 385 (1983).

[32] F. Verhulst, *Perturbation Analysis of Parametric Resonance*, edited by R. A. Meyers, Encyclopedia of Complexity and Systems Science (Springer, New York, 2011).

[33] F. Brau, H. Vandeparre, A. Sabbah, C. Poullard, A. Boudaoud, and P. Damman, Nat. Phys. **7**, 56 (2011).

[34] V. Petrov, Q. Ouyang, and H. L. Swinney, Nature **388**, 655 (1997).

[35] F. A. Döerfler, Dynamics and control in power grids and complex oscillator networks, Ph.D. thesis, University of California (Santa Barbara, 2013).

[36] B. A. M. Owens, M. T. Stahl, N. J. Corron, J. N. Blakely, and L. Illing, Chaos **23**, 033109 (2013).

[37] M. Kapitaniak, K. Czolczynski, P. Perlikowski, A. Stefanski, and T. Kapitaniak, Phys. Rep. **541**, 1 (2014).

[38] M. J. Clifford and S. R. Bishop, Phys. Lett. A **201**, 191 (1995).

[39] Xu Xu, M. Wiercigroch, and M P. Cartmell, Chaos Soliton Fract. **23**, 1537 (2005).

[40] S. Lenci, E. Pavlovskaia, C. Rega, and M. Wiercigroch, J. Sound Vib. **310**, 243 (2008).

[41] E. Pavlovskaia, B. Horton, M. Wiercigroch, S. Lenci, and C. Rega, Int. J. Bifurcat. Chaos **22**, 1250100 (2012).

[42] For a system subject to periodic perturbation of period T_p, the term "period-n" indicates the solution is periodic with period equal to nT_p.

[43] P. J. Bryant and J. W. Miles, J. Aust. Math. Soc. B **32**, 42 (1990).

[44] M. J. Clifford and S. R. Bishop, J. Aust. Math. Soc. B **37**, 309 (1996).

[45] S. R. Bishop and M. J. Clifford, Chaos Soliton Fract. **7**, 1537 (1996).

[46] B. P. Koch and R. W. Leven, Physica D **16**, 1 (1985).

[47] J. Guckenheimer and P. Holmes, *Nonlinear Oscillations, Dynamical Systems, and Bifurcations of Vector Fields*, 1st ed. (Springer-Verlag, New York, 1983).

[48] S. Wiggins, *Introduction to Applied Nonlinear Dynamical Systems and Chaos*, 2nd ed. (Springer-Verlag, New York, 2003).

[49] When the Melnikov method is applied to the vertically excited parametric pendulum, and also to other similar parametric systems, such as the parametric pendulum subject to nonharmonic excitation [50] and the pendulum with varying length [51], integrating Eq. (5), we see that the term that can lead to non simple zeros of the Melnikov integral is nonidentically null only for even oscillations. Thus, the parameter thresholds for the existence for odd oscillations cannot be computed, at least through this method.

[50] M. A. F. Sanjuán, Chaos Soliton Fract. **9**, 995 (1998).

[51] A. Belyakov and A. P. Seyranian, Nonlinear Dynam. **77**, 1617 (2014).

[52] K.-H. Kwek and J. Li, Int. J. Nonlinear Mech. **31**, 277 (1996).

[53] The natural frequency of oscillation f_0 was obtained by measuring the period of small oscillations, and the friction parameter b was obtained by following the natural decay of small oscillations.

[54] E. J. Doedel, Congr. Numer. **30**, 265 (1981).

[55] E. J. Doedel and B. E. Oldeman, *Auto-07p: Continuation and bifurcation software for ordinary differential equations*, Tech. Rep. (2007).

[56] See Supplemental Material at http://link.aps.org/supplemental/10.1103/PhysRevE.94.012202 for the numerical code to generate parameter spaces for the parametric pendulum using direct integration (instructions can be found in the README.txt file). Also see the videos *P1.avi*, *P4.avi*, and *P5.avi*, illustrating period-1, period-4, and period-5 oscillations, respectively, for $A = 2.02$ cm and $f_p = 7.95$ Hz, taped at 250 fps and shown at 25 fps.

[57] J. C. Sartorelli and W. Lacarbonara, Nonlinear Dynam. **69**, 1679 (2012).

[58] J. C. Sartorelli, B. Marin, F. A. C Pereira, A. Arena, W. Lacarbonara, ENOC - 8th European Nonlinear Dynamics Conference, Vienna, 2014 (unpublished).

[59] P. F. Byrd and M. D. Friedman, *Handbook of Elliptic Integrals for Engineeres and Physicists*, 1st ed. (Springer, Berlin, 1954).